JGS
Journal of the Geological Society

Research article

Published Online First

https://doi.org/10.1144/jgs2017-039

Repeated reactivation of clogged permeable pathways in epithermal gold deposits: Kestanelik epithermal vein system, NW Turkey

Nilay Gülyüz[1,2*], Zoe K. Shipton[1], İlkay Kuşcu[3], Richard A. Lord[1], Nuretdin Kaymakcı[4], Erhan Gülyüz[2] & David R. Gladwell[5,†]

[1] Department of Civil and Environmental Engineering, University of Strathclyde, Glasgow G1 1XQ, UK
[2] Department of Geological Engineering, Yüzüncü Yıl University, 65080 Van, Turkey
[3] Department of Geological Engineering, Muğla Sıtkı Koçman University, 48000 Muğla, Turkey
[4] Department of Geological Engineering, Middle East Technical University, 06800 Ankara, Turkey
[5] Geochemico Consulting Incorporated, 241021 Concession 3 Allenford, ON, N0H 1A0, Canada
[†] deceased
N.G., 0000-0002-1230-6950
* Correspondence: yagcioglu88@gmail.com

Abstract: This study presents a detailed study of the dimensions, geometry, textures and breccias of a well-exposed epithermal vein system, the Kestanelik gold deposit in the Biga Peninsula, NW Turkey, and investigates the permeability enhancement mechanisms in epithermal gold deposits. Here mineralization is associated with quartz veins up to 13.6 m thick. Vein textures and breccia components indicate repeated sealing and subsequent brecciation of wall rock and pre-existing vein infill. Field and petrographic analyses characterize east–west-trending veins as left lateral faults, whereas NE–SW-trending veins are extensional (Mode I) fractures. Cataclasite and tectonic breccia of wall rocks and early quartz, hydrothermal crackle breccias, and matrix-supported chaotic breccias of pre-existing vein infill, all of which are cemented by late iron-oxide-bearing quartz, indicate that co-seismic rupturing and hydraulic fracturing are two major permeability enhancement mechanisms. In addition, transient variations in local stress direction, caused by syn-mineralization dyke intrusion, may have enhanced permeability on misoriented surfaces and at locations where the dip changes. This study emphasizes the importance of understanding structural geology and kinematics as controls on the location of boiling and mineralization mechanisms in epithermal gold deposits.

Received 15 March 2017; **revised** 6 December 2017; **accepted** 6 December 2017

Epithermal deposits originate in the upper, brittle crust in regions with active magmatic and geothermal activity. Mineralization in these deposits is dominantly hosted by veins or stockworks, confirming that brittle fault and fracture systems play a major role in the circulation of hydrothermal fluids (Buchanan 1981; Hedenquist & Lowenstern 1994; Curewitz & Karson 1997). The ore and gangue minerals in the veins are typically the result of multiphase precipitation (Spurr 1925; Hulin 1929; Buchanan 1981; Sibson 1987; Hedenquist *et al.* 2000), and are associated with repeated and episodic fluid flow rather than a steady-state process (Sibson 1987; Micklethwaite & Cox 2004; Woodcock *et al.* 2007). Additionally, radiometric dating of some hydrothermal deposits indicates that permeability creation and hydrothermal fluid circulation could take place over thousands to tens of thousands of years (Fournier 1989; Lalou *et al.* 1993), or as long as millions of years in major porphyry systems (Sillitoe 2010). Understanding how subsequent permeability enhancement can be achieved after the deposition of minerals in fractures and faults chokes permeable pathways and restricts fluid flow is crucial.

Several mechanisms for precipitation from the circulating hydrothermal solutions are invoked for both high- and low-sulphidation epithermal systems, such as boiling, oxidation, fluid mixing, adiabatic boiling and pH change. The most favourable precipitation mechanism in low-sulphidation epithermal systems is boiling. Epithermal fluids rise from depth along structural pathways at high temperatures under suitable pressure to prevent boiling. When the pressure drops suddenly (e.g. through faulting- or fracturing-related dilation), boiling occurs. Even small-magnitude earthquakes ($M_w < 2$) can trigger boiling (Sanchez-Alfaro *et al.* 2016). Changes in the fluid chemistry by boiling result in precipitation of base metals at deeper levels, and precious ore and gangue minerals at relatively shallower depths until the open spaces are sealed, and fracture permeability is occluded or lost (Buchanan 1981; Henley 1985; Hedenquist *et al.* 2000).

The mineralogical and geochemical aspects of low-sulphidation (LS) epithermal systems are well known (e.g. Buchanan 1981; White & Hedenquist 1990, 1995; Hedenquist & Lowenstern 1994; Hedenquist *et al.* 2000; Sillitoe & Hedenquist 2003; Simmons *et al.* 2005). However, limited studies exist on the fluid flow and permeability enhancement mechanisms in LS epithermal veins. The existing studies generally focus on the effect and significance of geometric and mechanical aspects of the fault–fracture systems on the epithermal deposits. Terminations of faults and locations of multiple fault interaction are areas of high fracture density and connectivity and are therefore likely to localize high fluid flow (Curewitz & Karson 1997; Cox *et al.* 2001; Cox 2005). Observation from fossil epithermal deposits shows that epithermal mineralization is often located in dilational jogs within fault systems (Sibson 1987). Major faults can be either important barriers or conduits to fluid flow (Caine *et al.* 1996; Rowland & Sibson 2004), and the permeability may be nonuniform along the fault depending on the relationship between the variable strike of the fault and the orientation of the local stress direction (Micklethwaite *et al.* 2010). Permeability can also be developed or maintained along some fault segments because interconnected fractures and subsidiary faults form in the wall rocks where a damage zone occurs adjacent to a

fault core (Caine *et al.* 1996; Davatzes *et al.* 2005). The damage zone structures that are permeable may also change position over geological time (Woodcock *et al.* 2007; Burnside *et al.* 2013). Micklethwaite & Cox (2004, 2006) argued that if the event responsible for opening permeable pathways is an earthquake, although the permeability of the fault where the mainshock occurs may rapidly be lost owing to the precipitation of hydrothermal minerals, enhanced fluid flow may occur along the structures where aftershock ruptures focus and the location of these structures is predictable based on stress transfer modelling.

Rather than focusing on structural controls at the fault system scale, this study presents the dimensions, geometry, kinematics, textures and breccias of the veins. We examine the very shallowest levels of a well-exposed epithermal vein system at the Kestanelik gold deposit (Biga Peninsula, NW Turkey). Field and drill core data are used to understand the deformation mechanisms and kinematics of the vein system, specifically focusing on determining the origin of the fracture zones (a shear fracture or extensional fracture zone) along which the mineralization has occurred. Implications for the vein-scale permeability enhancement mechanisms and effective prospect evaluation in epithermal gold deposits are explored.

This study has revealed significant new microstructural evidence for reactivation along the vein–wall rock contact and associated permeability development and fluid flow after the veins were clogged. These findings support the few earlier studies of the permeability enhancement mechanisms and fluid flow in epithermal systems (e.g. Sibson 1987; Cox *et al.* 2001; Micklethwaite & Cox 2004; Micklethwaite 2009) but are also the first detailed textural studies of the permeability enhancement mechanisms. This study also emphasizes the importance of understanding structural controls and triggers for mineralization that are evident from structures and textures during the exploration of epithermal gold deposits.

Kestanelik epithermal gold deposit

The Kestanelik gold deposit is located in the Biga Peninsula, NW Turkey, *c.* 45 km NE of Çanakkale. Paleozoic metamorphic and ophiolitic basement rocks are cut by various Eocene to Miocene plutons and covered by Cenozoic volcanic and sedimentary rock units (Okay *et al.* 1996) (Fig. 1). Starting from the Middle Eocene, extensive magmatism prevailed in NW Turkey that changed in character from calc-alkaline to alkaline in the Middle Miocene (e.g. Altunkaynak & Genç 2008).

The gold mineralization in the Kestanelik deposit is associated with quartz veins that crop out over an area of nearly 2 km^2 (Fig. 2). The veins are hosted by Paleozoic mica schist (Okay *et al.* 1990) and quartz–feldspar–hornblende (QFH) porphyry that yielded an age of 43.34 ± 0.85 Ma (K-feldspar Ar–Ar age) at the Madendağ low-sulphidation deposit (Ünal-İmer *et al.* 2013) *c.* 45 km to the SW of the Kestanelik deposit. The oldest sedimentary rock unconformably covering the mineralized veins is Priabonian limy sandstone, and the youngest host rock for the veins is the QFH porphyry. We therefore presume that the age of the mineralization is Late Lutetian–Early Priabonian (Middle to Late Eocene), suggesting that the Kestanelik gold deposit has a genetic link with the Eocene calc-alkaline magmatism in the region.

The Kestanelik epithermal gold deposit is an LS epithermal type. Classification as an LS epithermal system is based on the vein-ore textures, and predominant ore and gangue mineralogy. Although we have not identified adularia, a common mineral in low-sulphidation systems, pseudo-bladed quartz replacing bladed carbonate mineral is typical in LS systems. We also observed colloform to crustiform quartz, comb to cockade ore-vein textures, and hydrothermal breccias. Ore minerals are native gold and accessory silver. Quartz veins generally have moderate to high gold grades (Au range in 1–20 g t^{-1}) and the Au:Ag ratio is generally in the range of 2:1 to 1:1. Gangue minerals are principally quartz, amethyst and chalcedony with pyrite and accessory chalcopyrite, sphalerite and galena dissemination in the vein quartz.

Vein quartz textures observed in the field are types typically ascribed to open space filling (such as cockade and comb textures) and replacement (such as saccharoidal and pseudo-bladed textures). The most striking feature of the veins is brecciation. Quartz vein breccias are generally composed of monomictic to polymictic clasts of host rocks and/or earlier phase(s) cemented by quartz–iron oxide. Clasts of earlier breccia within some breccias indicate that at least two phases of brecciation occurred in the area. The absence of silica sinter, a diagnostic palaeosurface indicator in LS epithermal systems, suggests that the uppermost parts of the epithermal system have been eroded.

The QFH porphyry in the field area is always altered with some typical argillic alteration minerals (illite and smectite). These

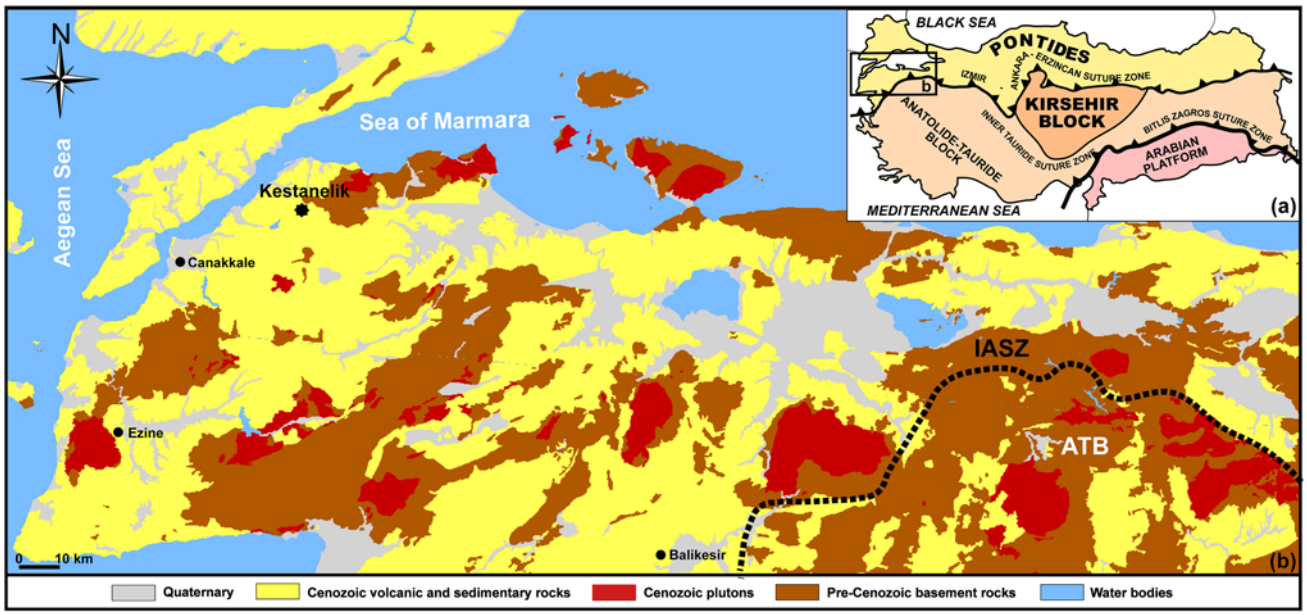

Fig. 1. (**a**) Major tectonic divisions of Turkey (simplified from Okay & Tüysüz 1999). (**b**) Simplified geological map of the Biga Peninsula with the location of the study area (modified from Türkecan & Yurtsever 2002).

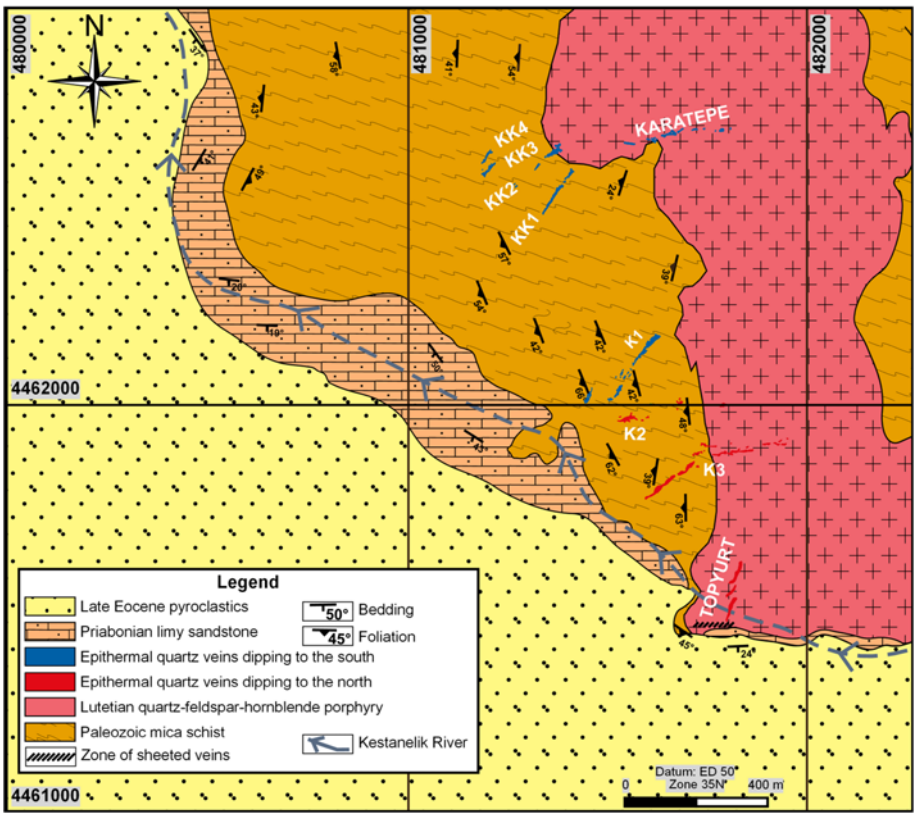

Fig. 2. Geological map of the study area, Kestanelik deposit.

assemblages were also observed in initial PIMA analyses (Hedenquist 2011). Alteration is more intense around field exposure and drill core samples of the veins, suggesting that the veins were the source of the alteration fluids. In deeper drill cores the degree of alteration is lower. All of the observed porphyry outcrops are altered; the furthest is up to 500 m away from the nearest observed vein. This is very wide for a vein-associated alteration halo (more typically a few tens of metres; Hedenquist *et al.* 2000).

A mafic dyke that cuts and contains fragments of altered QFH porphyry (xenoliths) is observed in a drill core. Adjacent to the dyke, a polymictic breccia contains clasts of the same dyke and vein quartz in turn cemented by quartz. This textural evidence indicates that the vein-related alteration was already present when the dyke was intruded, suggesting contemporaneous mineralization and dyke intrusion (Fig. 3). This dyke is therefore likely to be related to Cenozoic magmatism in the Biga Penninsula (e.g. Altunkaynak & Genç 2008).

The field area is cut by the deeply incised Kestanelik River, providing a topographic exposure interval of *c.* 150 m. The post-mineralization limy sandstone records a mean dip of 29° and direction of 110° to the SW. This tilting, coupled with the effect of the river incision, means that the NE flank of the valley is equivalent

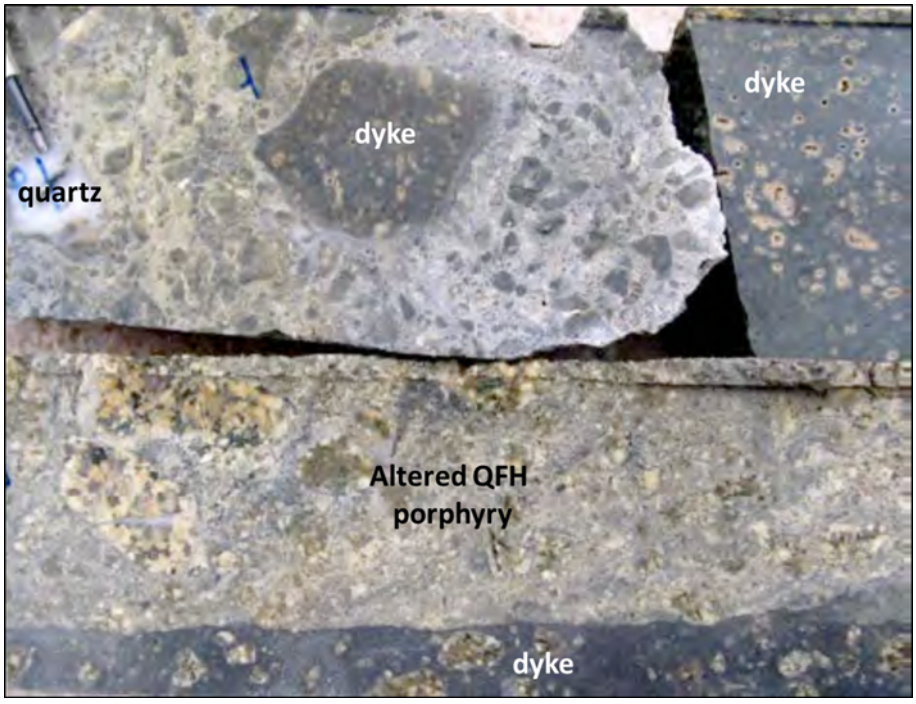

Fig. 3. A drill core (KED-6 65.5–65.7 m) photograph showing a mafic dyke (upper right) and adjacent breccia with fragments of dyke and quartz vein cemented by quartz (upper left) on the margin of altered QFH porphyry intruded by the dyke (bottom) indicating contemporaneous mineralization and dyke intrusion.

Table 1. *General characteristics of major quartz veins; all data are from measurements on outcrop*

Vein	Host rock	Number of data	Mean strike	Mean dip	Dip direction	Strike length (m)	Minimum width (m)	Maximum width (m)
Karatepe	QFH porphyry	23	084.2	69.8	SSE	350	0.8	8
KK1	Schist	11	047.3	76.7	SE	150	1.2	9
KK2	Schist	13	044.5	75.8	SE	185	1	8.5
KK3	Schist	5	046.9	70.2	SE	52	2	8.7
KK4	Schist	4	042.4	68.3	SE	47	1	5.8
K1	Schist	15	039.6	75.1	SE	240	0.9	13.6
K2	Schist	8	268	43.5	NNW	86	0.6	12.9
K3E	QFH porphyry	18	274.5	71	NNE	280	0.6	7.8
K3W	Schist	16	237.3	62.3	NW	230	2	12.5
Topyurt	QFH porphyry	10	224.5	65.1	NW	154	2	10

to a pseudo cross-section through the very shallowest part of the hydrothermal system with the palaeo-depth of vein emplacement increasing slightly to the SW of the field area.

Characteristics of the epithermal vein system

The gold mineralization in the area is hosted by major quartz veins, wall rock veins and sheeted veins in the river valley. Outcrop geometries of the veins were mapped using a Trimble GPS system (±0.1 cm). Vein-related detailed structural data (attitude, thickness, infill type, length and typology) were collected from surface exposures and outcrops along the creeks. The structural data were plotted using the software package Stereonet (Allmendinger *et al.* 2013; Cardozo & Allmendinger 2013) and used to calculate the palaeostress field at the time of gold mineralization. In addition, observations were made of the host rock deformation around the veins both in the field and in diamond-cut drill cores. Vein textures and breccias were examined both on exposed vein outcrops and in drill cores, with the help of petrographic analysis.

The 3D subsurface geometries of the vein–host rock boundaries were constructed by using mapped outcrop geometries, detailed field data, well-logs and geochemistry data from 396 drill holes (255 diamond-cut and 141 reverse circulation holes) supplied by Chesser Resources, who, at the time of fieldwork, were the licence holder company of the Kestanelik deposit. Modelling of the top and bottom surface of each vein was performed in MOVE Structural Modelling and Analysis Software granted by Midland Valley's Academic Software Initiative. In addition, vertical cross-sections perpendicular to the vein strike were created for each vein in the MOVE Software. All veins were modelled except two (the K2 and Topyurt veins), which had insufficient drillhole data.

Major quartz veins

There are nine major mineralized quartz veins that form a NW–SE-trending corridor in the deposit area. These veins, from north to south, are the Karatepe, KK4, KK3, KK2, KK1, K1, K2, K3 and Topyurt veins (Fig. 2). The host rock, strike length, mean strike, mean dip angle, and minimum and maximum width of each vein from outcrop measurements are summarized in Table 1. There are two mineralized vein sets in the area based on strike orientation; the first set strikes NE–SW (KK1, KK2, KK3, KK4, K1, western end of K3, Topyurt) whereas the second one trends east–west (Karatepe, K2, eastern end of K3). All of the veins are continuous (not segmented) except the segmented K3 vein and Topyurt veins; however, some veins have discontinuous outcrop traces owing to the erosion. The NE–SW sets host the majority of gold mineralization according to the average gold grade calculations of the modelled veins using the geochemical gold assay data of related drill cores (Table 2). We describe these veins in turn from north to south, representing veins emplaced at increasing palaeo-depths.

The Karatepe vein is located in the northern part of the area and is hosted entirely within the QFH porphyry. It is east–west oriented and extends for a strike length of 350 m. The vein dips to the south

Table 2. *Descriptive statistics of modelled surfaces of each vein. All data are from the vertices of the subsurfaces)*

Vein	Subsurface*	Number of vertices	Mean		Standard deviation		Median		Average gold grade ($g\ t^{-1}$)†
			Strike	Dip	Strike	Dip	Strike	Dip	
Karatepe	FW	110 847	091.9	55.9	26.3	8.5	085.8	56.3	0.461
	HW	26 048	092.7	55.8	25.1	10.9	085.8	57.3	
KK1	FW	7019	056.5	60.4	13.5	6.5	054.8	59.1	3.356
	HW	6202	055	62.6	6.4	5.1	054.9	61.8	
KK2	FW	444 923	065.7	51.8	11.8	4.6	066.3	52.1	2.081
	HW	341 583	067.5	53.2	16.4	8.6	065.8	55.8	
KK3	FW	45 065	065.1	61.1	16.5	3.9	065.3	61.6	3.484
	HW	52 235	055.7	66.2	9	4.1	055.7	66.2	
KK4	FW	231 999	056.6	57.5	7.9	3.8	056.8	58.3	0.866
	HW	209 578	058.3	59.9	5.2	3	058.4	60.5	
K1	FW	502 776	052.9	63.6	22.8	6.8	050.3	64.7	2.921
	HW	384 859	052.9	67.5	19.8	7.6	049	68.7	
K3E	FW	1 048 569	261.9	66.4	29	17	264.9	70.2	1.326
	HW	1 042 016	261	69	29.6	16.6	266.1	72.4	
K3W	FW	439 652	225.9	63.3	31.9	8	232.3	64.4	6.943
	HW	317 971	227.8	64.5	31.3	8.9	234.1	66.4	

*FW, footwall; HW, hanging wall. As is common in the mining literature we use these terms to refer to the wall below and above the vein respectively, and not to imply kinematics.
†Average gold grade values are calculated based on the geochemical gold assay data from the drill cores of the modelled veins.

(Fig. 2) with an average dip of 69.8° (from surface data; subsurface dips are given in Table 2). Vein orientation data collected from outcrop revealed that the vein has a very corrugated strike on a metre scale. The deepest drill intersection is around 160 m below surface.

The KK3 and KK4 veins are hosted by mica schist and strike almost NE–SW (Fig. 2). KK3 vein has a 52 m strike length and varies between 2 and 8.7 m wide. The vein dips to the SE with an average dip of 70.2°. The KK4 vein has a strike length of 47 m and dips to the SE with an average dip of 68.3°. The deepest drill intersection of the KK3 and KK4 veins is around 120 and 100 m below surface, respectively.

The KK1 vein and KK2 vein are hosted by mica schist and trend approximately NE–SW (Fig. 2). The KK1 vein extends 150 m along-strike and dips to the SE with an average dip of 76.7°. Vein outcrop width varies between 1.2 and 9 m. The KK2 vein outcrop extends for 185 m, with an average dip of 75.8° to the SE. The deepest drill intersection of the KK1 and KK2 veins is around 125 and 100 m below surface, respectively.

The NE–SW-trending K1 vein extends over a strike length of around 240 m and dips to the SE (Fig. 2) with an average dip of 75.1°. The deepest drill intersection is around 90 m below surface.

The K2 vein, hosted by mica schist, has an east–west-trending strike length of 86 m and dips gently to the north (Fig. 2) with an average dip of 43.5°.

The K3 vein is composed of two segments and its strike extends over 510 m (Fig. 2). The western segment of the vein system (K3W vein) is hosted by mica schist and trends NE–SW with a strike length of 230 m (Fig. 2). It dips to the NW with an average angle of 62.3°. The deepest drill intersection is around 215 m below surface. The eastern segment of the vein system (K3E vein) is hosted by the QFH porphyry, extends intermittently over an east–west-oriented corrugated strike with a length of 280 m and dips to the north (Fig. 2) with an average angle of 71°. The deepest drill intersection is around 140 m below surface. The western segment of the K3 vein is more persistent and thicker than its eastern part.

The Topyurt vein, hosted by QFH porphyry, is located in the southern part of the study area perpendicular to the valley and cuts the Kestanelik River. It has three subparallel NE–SW-trending segments in an north–south-trending zone (Fig. 2) with a total exposed strike length of 154 m and dips to NW with an average dip of 65.1°.

The host rock, strike length, mean strike, mean dip, and minimum and maximum width of each vein are summarized in Table 1.

The top and bottom surfaces of major quartz veins modelled in three dimensions (Fig. 4a) indicate that the thickness of the veins decreases with depth and that the veins generally have a flaring upwards geometry (Fig. 4b). The attitude of the modelled vein surfaces is generally different from that observed in vein outcrops (compare Tables 1 and 2) as the veins change geometry with depth (Fig. 4b). Histograms of the subsurface dip data of the modelled veins show that the dominant subsurface dip angle of each vein is close to that measured at the surface. In addition, rose plots of the subsurface strike data indicate that the dominant subsurface strike of each vein is close to that at the surface (Table 1 and Fig. 4c), although there are not many measurements from the surface owing to erosion along vein walls (Table 1). The mapped variable geometry along-strike is mirrored at depth and most of the veins have multiple locations at depth where the dip changes (i.e. the veins have vertically segmented sections with differing dips) (Fig. 4b). East–west-trending veins have more geometric irregularities than NE–SW-trending ones both along-strike and along-dip (Fig. 4c and Table 2; see standard deviation values).

In layered rocks such dip segmentation has been previously interpreted to be the result of the competency contrast within different host rocks (e.g. Schöpfer *et al.* 2006, 2007). However, at this site the dip segmentation appears to be independent of the host rock type. Segmentation in the dip direction may also be caused by the growth and coalescence of small planar segments of the structures (whether faults or open-mode fractures) (Cox 2005).

Wall rock veins

Detailed structural data (thickness, infill type, length, attitude and typology) were collected from the wall rock structures surrounding two of the major mineralized quartz veins: the Karatepe vein and the Topyurt vein. Dense vegetation and thick soil cover around other vein-associated structures prevented the collection of structural data.

The east–west-trending Karatepe vein is associated with an array of extensional veins in the wall rock, which define left-lateral kinematics (Fig. 5a). These veins have comb-textured hydrothermal quartz crystals oriented perpendicular to the vein walls (Fig. 5b and c). Their width varies between 4 and 26 cm. Their orientations are given in Figure 5d. The wall rock veins in drill core define a complex mesh of multiple fracture orientations with mutual cross-cutting relationships (Fig. 6a and b) indicating several episodes of fracturing in the damage zone to the main veins.

The Karatepe wall rock also contains veinlets that are too thin to be visible in hand specimen. The petrographical studies showed that the veinlets are filled by inequant granular hydrothermal quartz (Fig. 6c). This texture shows that the opening of the fracture was more rapid than the growth of the quartz crystals (Ramsay 1980; Woodcock *et al.* 2007).

The area surrounding the Topyurt vein system is also dominated by extensional veins (Fig. 7a). These veins are observed only in the footwall of the Topyurt vein (the hanging wall is not exposed) (Fig. 7a) and their width varies between 3 and 20 cm on the surface. They are characterized by the same infill of hydrothermal quartz and have comb-textured hydrothermal quartz crystals oriented perpendicular to the vein walls (Fig. 7b). A stereonet of their orientation data is presented in Figure 7c. The NE–SW-trending Topyurt vein components and its wall rock structures are consistent with a right-lateral en echelon brittle shear zone.

Sheeted quartz veins

Sheeted quartz veins hosting epithermal mineralization are present along the Kestanelik River valley in the southern part of the study area (Fig. 2). These closely spaced, subvertical and subparallel veins are oriented almost perpendicular to the course of the river bed, hosted by QFH porphyry (Fig. 8a) and form up to 25% of the total rock volume. Their thicknesses vary between 0.5 and 15 cm (Fig. 8b and c). They therefore cannot be shown individually on the map, and the region where they crop out has been indicated by shading (Fig. 2). Although outcrop quality is variable across the area, similar veins are seen nowhere else, so they appear to be confined to the deep levels of the vein system where exposed in the deeply incised river valley.

These steeply dipping veins contain well-developed hydrothermal quartz crystals almost perpendicular to the vein walls (Fig. 8c), and there is no evidence of shearing along the vein walls; therefore they are very likely to be extensional veins. Attitude data recorded from these veins are shown on a stereonet (Fig. 8d).

Vein textures and breccias

The epithermal quartz veins at the Kestanelik deposit are dominated by the textures resulting from the boiling of hydrothermal fluids, such as cockade (Fig. 9) and colloform (Fig. 10b) textures indicative of open space filling characteristics, and textures representing replacement such as pseudo-bladed and saccharoidal (e.g. Buchanan 1981; White & Hedenquist 1990; Dong *et al.* 1995). Colloform texture at Kestanelik refers to fine rhythmic bands of

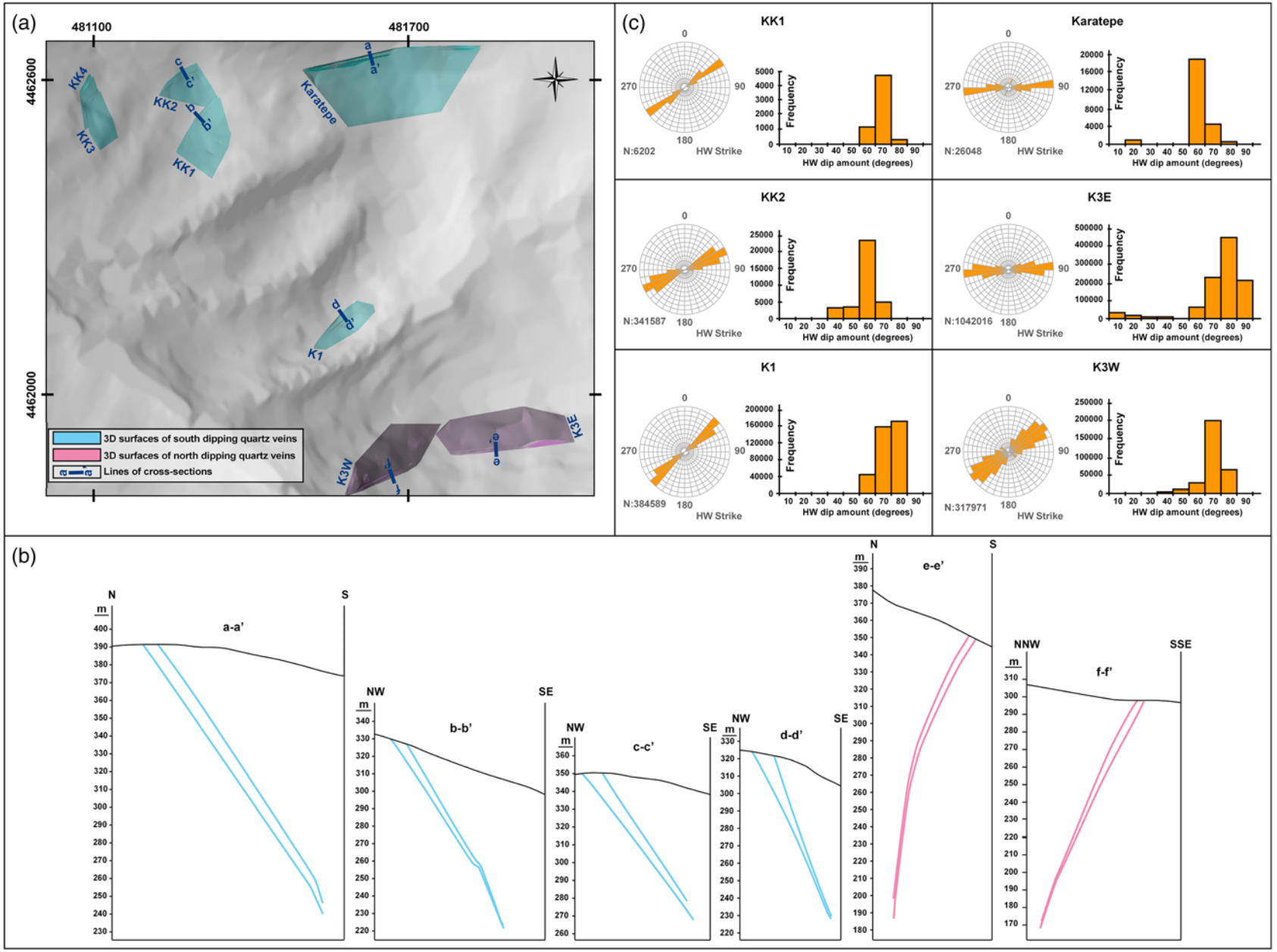

Fig. 4. (**a**) A 3D view of modelled top and bottom surfaces of major quartz veins with digital elevation model. (**b**) Representative cross-section of each vein showing the flaring upwards geometry of the veins and their decreasing thickness with depth. (**c**) Rose plot of strike values and histogram of dip amount values of hanging-wall surfaces of each vein showing the strike and dip variability of modelled surfaces.

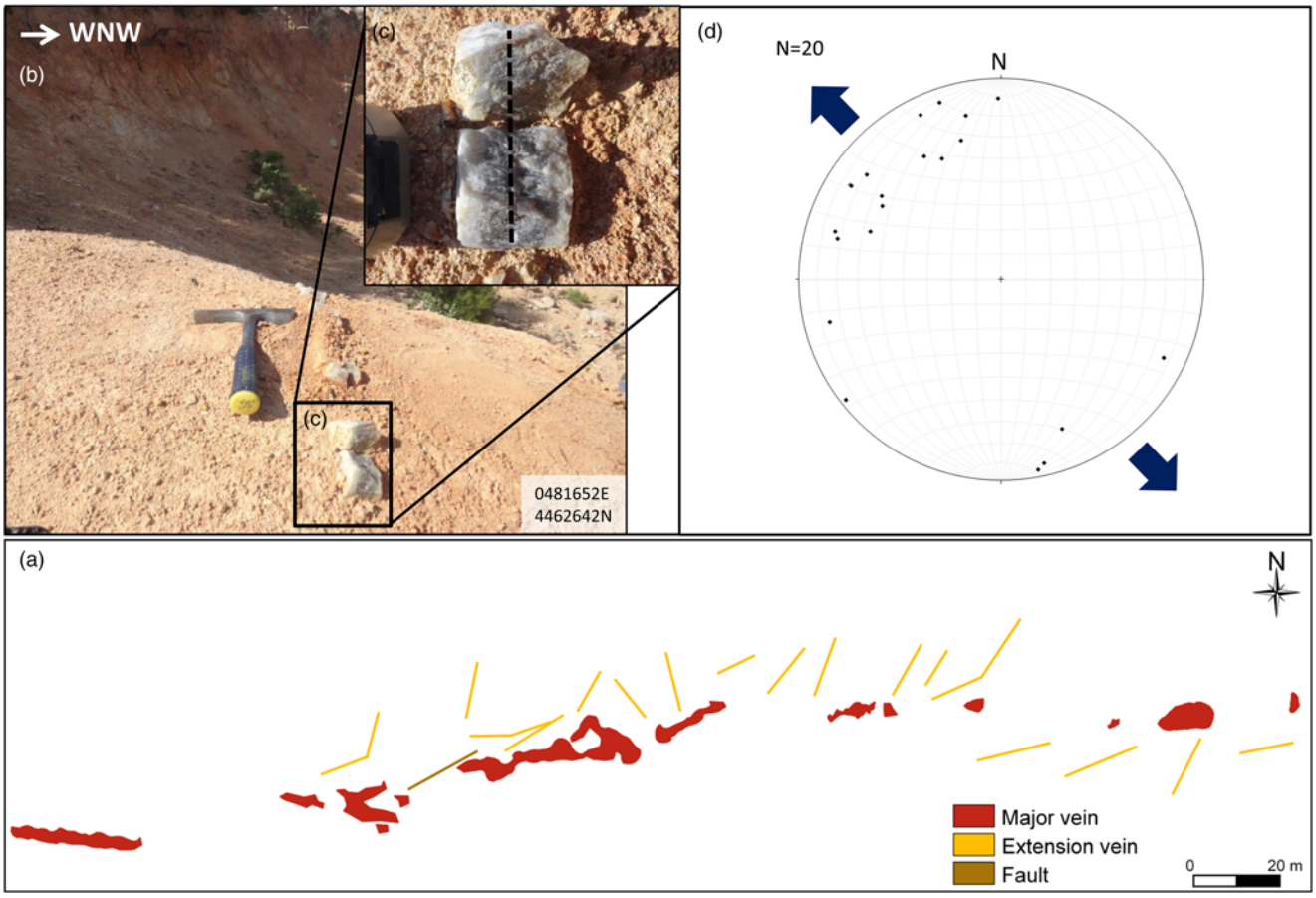

Fig. 5. (**a**) Detailed map of the Karatepe vein and its wall rock veins. (**b**) Photograph showing one of the extension veins around the Karatepe vein. (**c**) Closer view of the extension vein with comb-textured hydrothermal quartz. (**d**) Poles to the extensional veins around the Karatepe vein plotted on an equal-area stereonet with the arrows indicating the opening direction for the veins.

chalcedony (Fig. 10b). Cockade texture forms when isolated fragments of wall rock or early vein material are rimmed by fine-grained rhythmic bands of quartz (Figs 9 and 10b). Pseudo-bladed texture forms when quartz or chalcedony aggregates replace bladed or platy calcite along their original crystal outlines (Fig. 11b–h) immediately after the boiling and removal of CO_2. Saccharoidal texture occurs when quartz replaces the massive granular carbonate along crystallographic defects, and in this texture loosely packed vitreous to milky fine-grained quartz aggregates show sugar appearance in hand specimen (Figs 11a–e and 12).

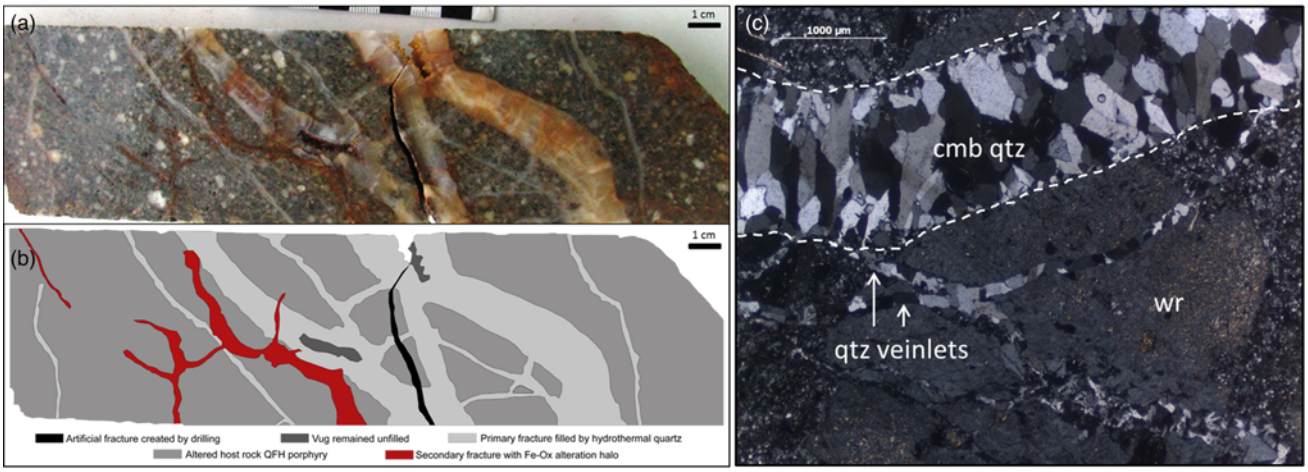

Fig. 6. (**a**) A core sample from KED-18 133.8–134 m showing mutual cross-cutting relationships of the wall rock veins close to the Karatepe vein footwall–wall rock contact (1.2 m from the vein wall down-hole equivalent to 0.9 m perpendicular distance) at the footwall of the vein. It should be noted that the host porphyry here is not as altered as it is higher in the section, where is has a strong yellow alteration (Fig. 5). (**b**) Sketch of the core sample. (**c**) A comb quartz veinlet filled by inequant granular hydrothermal quartz, and thinner quartz veinlets traversing the clay altered wall rock QFH porphyry close to the Karatepe vein footwall margin showing that opening rate of the fracture is greater than the precipitation rate of the cement (cmb qtz, comb quartz; wr, wall rock) (KED-16 124.4 m) (crossed polars image).

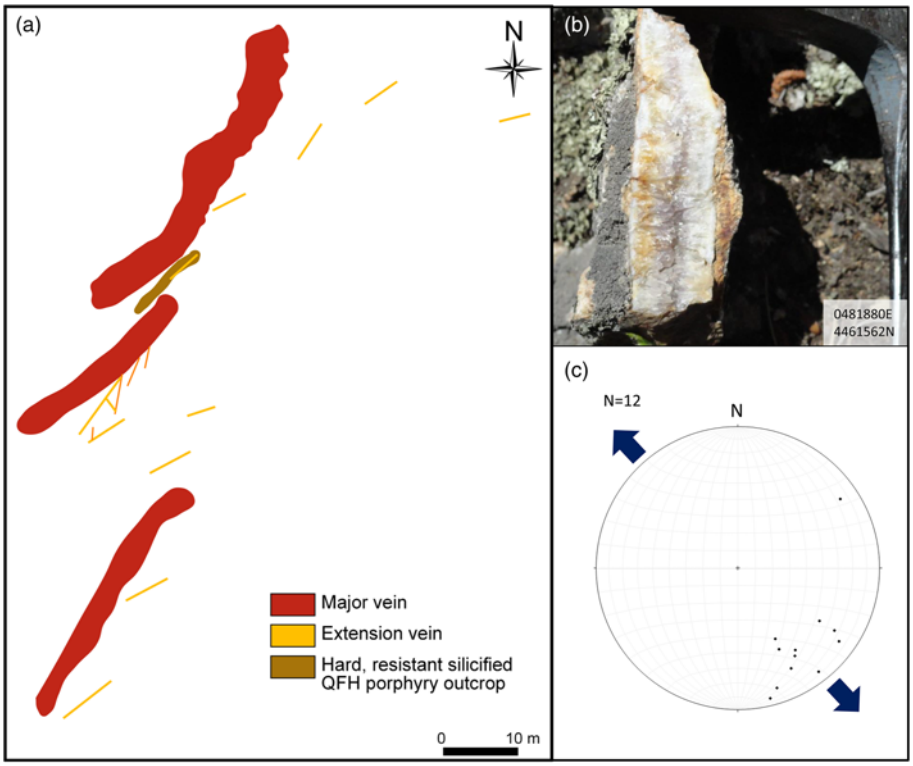

Fig. 7. (**a**) Detailed map of the Topyurt vein and its wall rock veins. (**b**) Photograph showing one of the extension veins with comb-textured hydrothermal quartz around the Topyurt vein. (**c**) Poles to the extensional veins around the Topyurt vein plotted on an equal-area stereonet with the arrows indicating the opening direction for the veins.

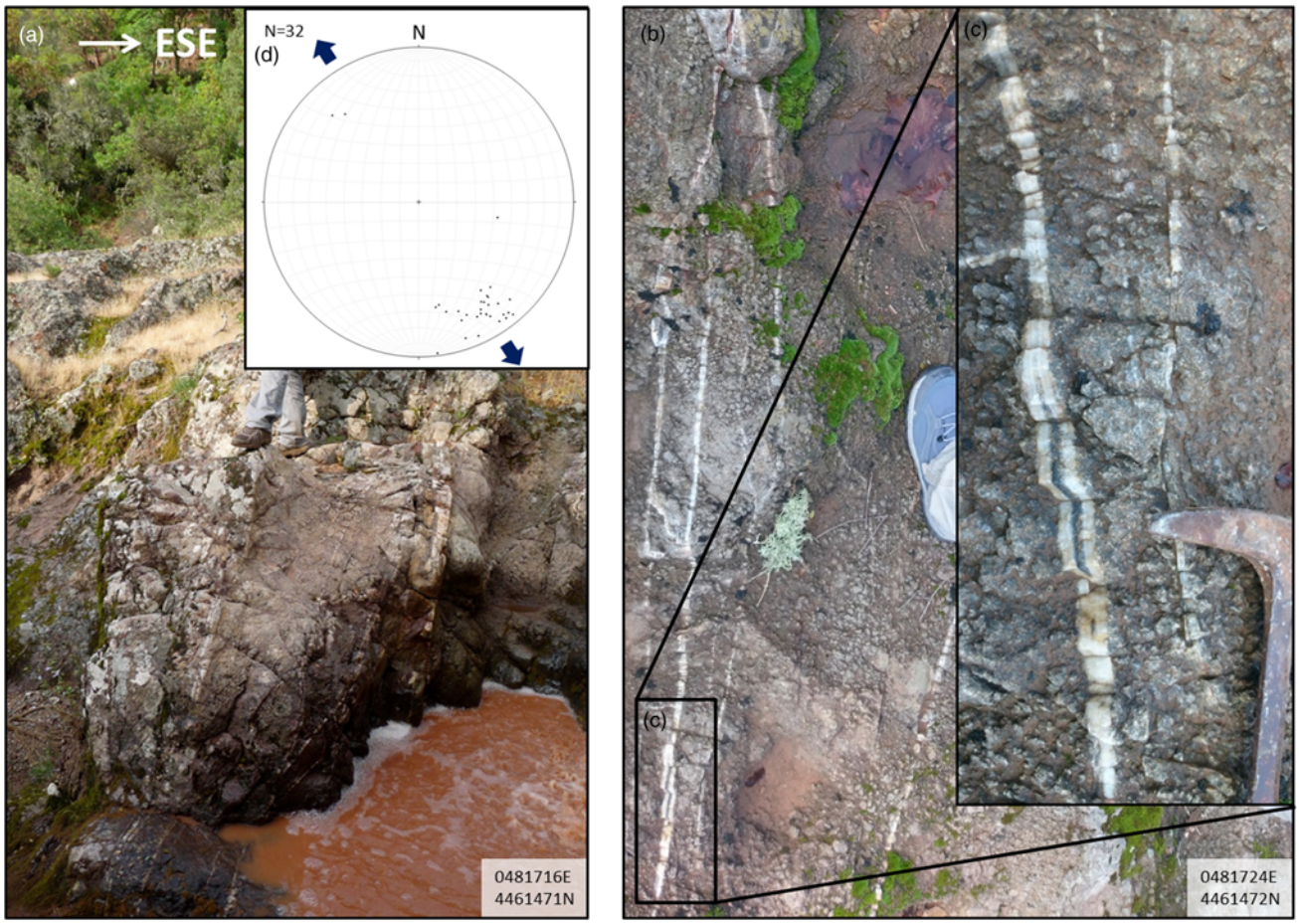

Fig. 8. (**a**) Photograph showing the subvertical and subparallel sheeted quartz veins along the Kestanelik River valley. (**b**) Photograph showing some of the sheeted quartz veins. (**c**) Closer view of one of the sheeted extensional veins with comb-textured well-developed hydrothermal quartz crystals oriented perpendicular to the vein walls. (**d**) Poles to the sheeted quartz veins plotted on an equal-area stereonet with the arrows indicating the opening direction for the veins.

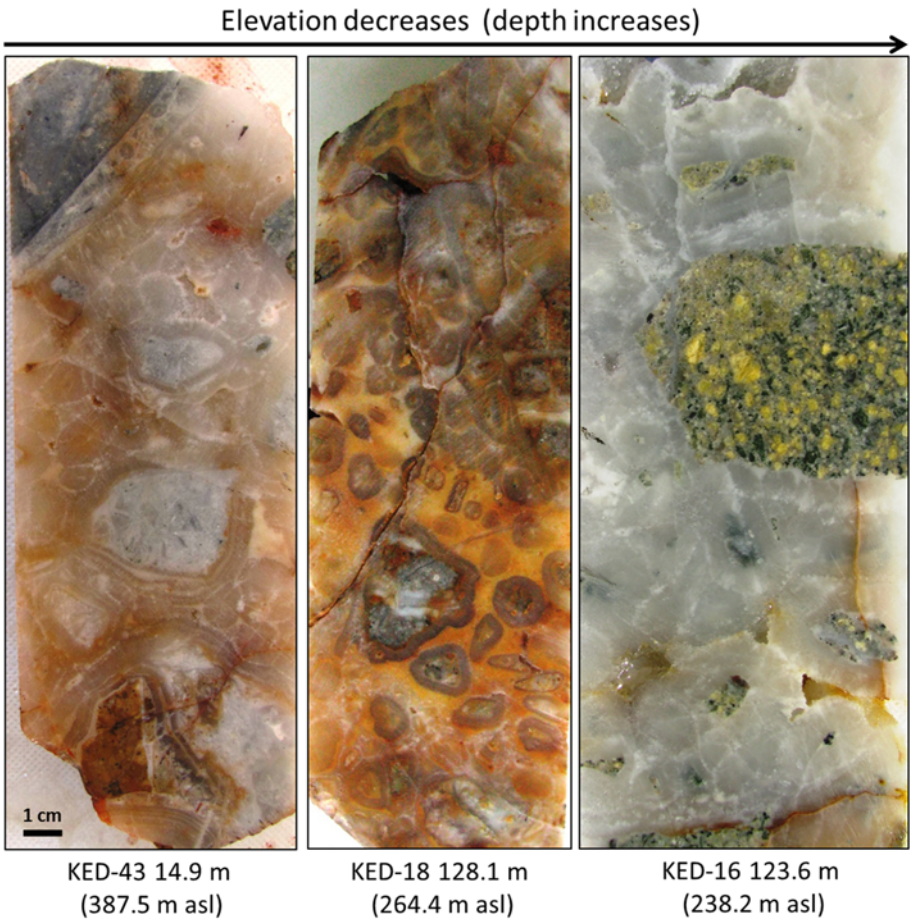

Fig. 9. Cockade breccias composed of chalcedony enclosing subrounded to rounded and poorly sorted clay altered QFH porphyry clasts at different levels of the Karatepe vein. Size of individual cockade breccias neither decreases nor increases as elevation decreases (it should be noted that the scale is the same for each photograph).

Although the Karatepe vein is dominated by chalcedony, other veins are characterized by quartz infill. The most striking feature of the veins is brecciation suggesting multiple generations of hydrothermal fluid flow and mineralization. All the major veins are brecciated except the Karatepe vein (Table 1). The sheeted veins are not brecciated, although they can display two generations of fills (Fig. 8c).

The Karatepe vein is dominated by breccias with cockade texture hosted by altered QFH porphyry. Wall rock clasts within the cockade breccia are subrounded to rounded and poorly sorted. This shows that the vein was emplaced along a zone that was already brecciated before the first phase of fluid flow. The clasts show neither normal nor reverse grading in any of the drill cores from all depths of the vein (Fig. 9).

A cataclasite of feldspar (from the wall rock QFH porphyry) and early chalcedony (Fig. 10a) cemented by a relatively later (younger) phase of chalcedony was observed by the petrographic study of a thin section from a drill core sample (Fig. 10b) taken from the footwall of the Karatepe vein–wall rock contact. This cataclasite indicates that after the vein was sealed owing to a first phase of fluid flow and associated mineralization, further shearing occurred along the vein footwall–wall rock contact, producing cohesive cataclasite.

All veins except the Karatepe vein are cement-supported, monomictic to polymictic breccias composed mostly of clasts derived from host rocks, which are mainly schist, and/or pre-existing quartz veins cemented by quartz or quartz–iron oxide (hematite and/or goethite). Four breccia types were recognized on the basis of

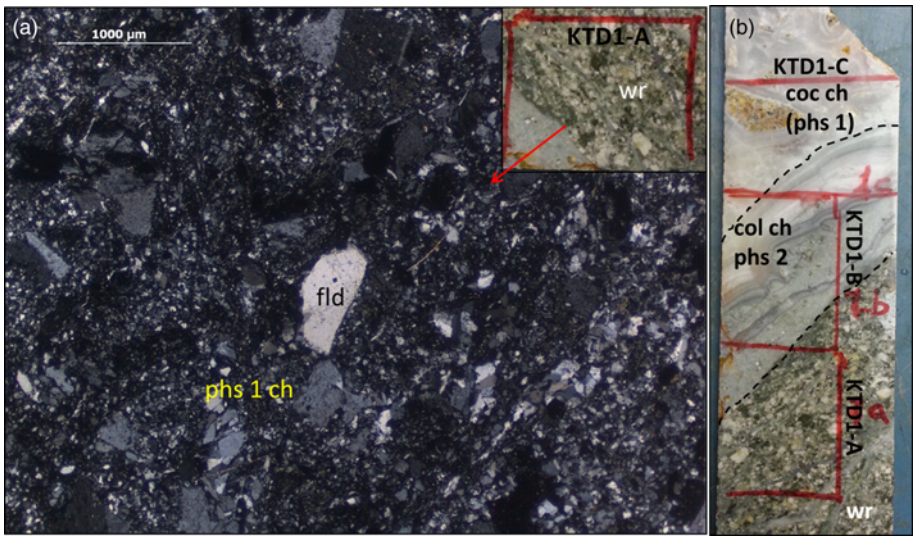

Fig. 10. (**a**) Cataclasite of feldspar (from the wall rock QFH porphyry) and early (phase 1) chalcedony (crossed polars image). It should be noted that drill cores are not oriented so it is not possible to derive the sense of slip. (**b**) Photograph of the drill core sample (KED-16 at 124.2–124.4 m) taken from the footwall of the Karatepe vein–wall rock contact showing the thin section location at which cataclasite was observed and two textures representing two mineralization phases of the vein (fld, feldspar; ch, chalcedony; col ch, colloform chalcedony; coc ch, cockade chalcedony; wr, wall rock).

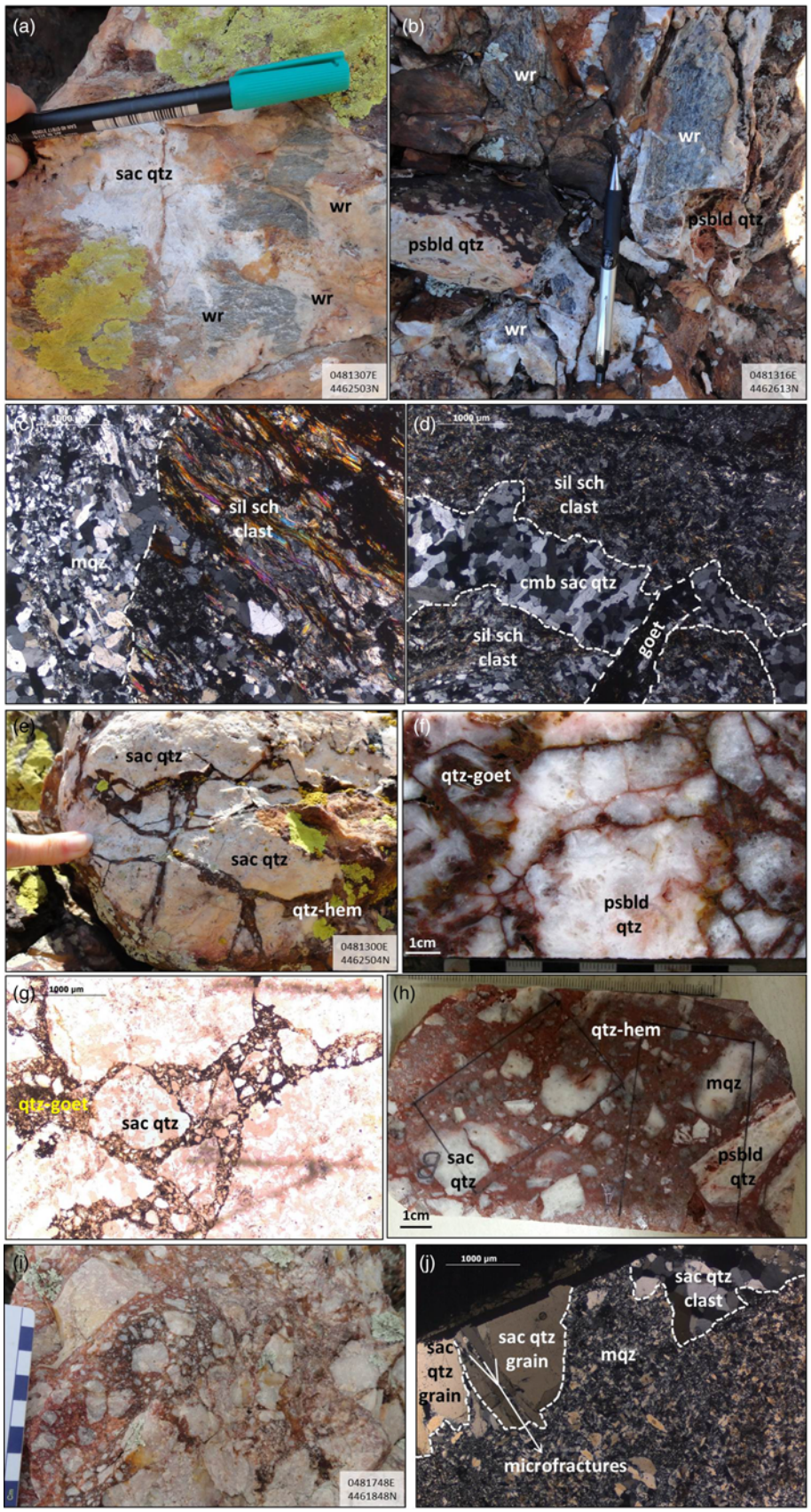

Fig. 11. (**a**) Breccia with clasts of wall rock schist plus a cement of saccharoidal quartz close to the hanging wall of the KK1 vein. (**b**) Breccia with clasts of wall rock schist plus a cement of pseudo-bladed quartz close to the hanging wall of the KK2 vein. (**c**) Breccia with schist clast (it should be noted that the silicification is after brecciation, and that matrix and foliation planes are in optical continuity) (K3 vein) (crossed polars image). (**d**) Comb quartz matrix between two clasts of silicified schist. Silicification is parallel to foliation and before comb qtz formation (KK1 vein; crossed polars image). (**e**) Crackle breccia with the clasts of saccharoidal quartz separated by quartz–hematite cement observed close to the margin of KK1 vein. (**f**) Crackle breccia with the clasts of pseudo-bladed quartz separated by quartz-goethite cement observed in a drill core cutting the K3 vein (KED-14 70.5–70.65 m). (**g**) Crackle breccia with clasts of saccharoidal quartz cemented by quartz–goethite in a drill core cutting the KK1 vein (KED-7 13.1–13.2 m). (**h**) Chaotic breccia composed of polymictic clasts of pre-existing vein infill with different quartz textures cemented by quartz–hematite in a drill core cutting the K3 vein (KED-20 30.1–30.2 m). (**i**) Chaotic breccia composed of polymictic clasts of pre-existing vein infill with different quartz textures cemented by quartz–hematite from the upper levels of the K3 vein outcrop. (**j**) Tectonic breccia with deformed clasts and grains of early saccharoidal quartz set in a microcrystalline quartz matrix observed in a thin section made from a hand sample taken from the outcrop of the K3 vein footwall margin (it should be noted that the microcrystalline quartz replaces saccharoidal quartz fragments along the microfractures) (crossed polars image). sac qtz, saccharoidal quartz; psbld, pseudo-bladed quartz; wr, wall rock; mqz, microcrystalline quartz; sil sch, silicified schist; cmb sac qtz, comb-textured saccharoidal quartz; goet, goethite; qtz-hem, quartz–hematite; qtz-goet, quartz–goethite.

macroscopic and microscopic observations from the vein outcrops and drill cores, as follows.

(1) Cement-supported breccias comprise host rock clasts, most commonly schist, cemented either by saccharoidal or pseudobladed quartz, or by crystalline quartz. The poorly to well-sorted clasts are angular to sub-angular, and the cement is more than 50% of the rock volume. These breccias are generally observed close to the vein margins and form semi-continuous domains on the exposed vein outcrops (Fig. 11a and b). Schist clasts commonly have silicification between foliation planes. In Figure 11c, foliation-parallel silicification is synchronous with the silica forming the breccia cement: silica at the contact of the clast with the cement can be seen to be in optical continuity with the foliation-parallel silica.

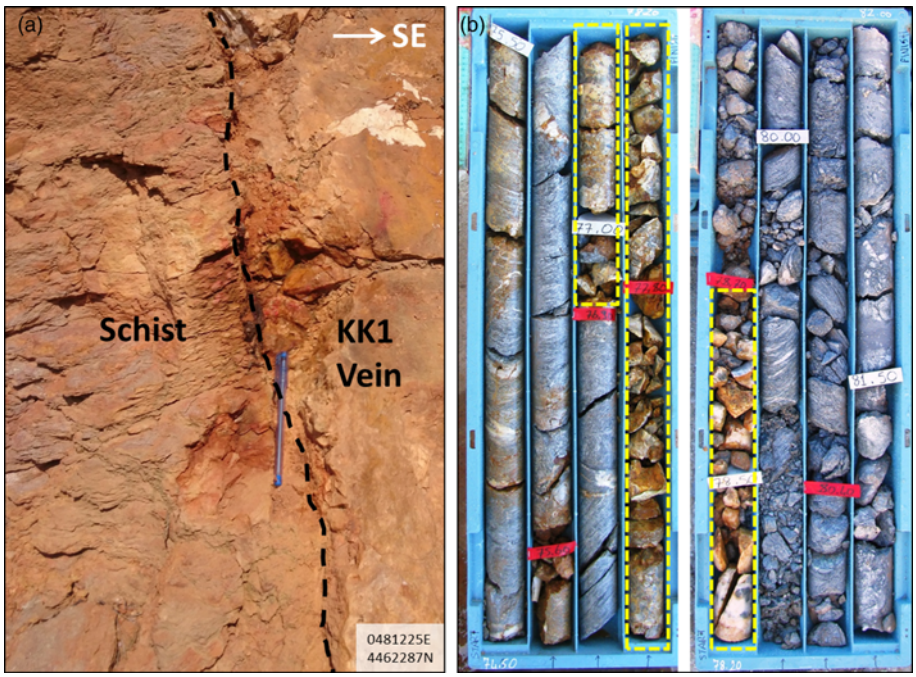

Fig. 12. (**a**) Sharp contact between the footwall of the KK1 vein and wall rock schist. (**b**) Photograph of KED-105 74.5–82 m interval core boxes showing that the foliation of the schist does not change around the K1 vein. It should be noted that the white veins around the K1 vein interval generally observed parallel to the foliation planes include meta-quartz (dashed lines indicate the vein interval).

Conversely, in Figure 11d, clasts containing foliation-parallel silicification are surrounded by a later quartz cement.

(2) Crackle (jigsaw-fit) breccias consist of clasts of pre-existing vein infill that generally match together and are cemented by quartz–hematite or quartz–goethite in a network of veinlets. Moderately to well-sorted clasts are generally angular to sub-angular. In these cement-supported breccias, the cement is always less than 50% of the rock volume (Fig. 11e–g).

(3) Chaotic breccias are composed of polymictic clasts of host rock and/or pre-existing vein infill with different quartz textures. The cement is quartz–hematite or quartz–goethite. Clasts are sub-angular to angular, poorly to well-sorted, and range from millimetre to centimetre scale. These breccias are generally more frequent at the highest part of the vein outcrops (Fig. 11h and i).

(4) Tectonic breccias with shear indicators were seen only in two thin sections made from K3 vein and provide evidence that the east–west-trending K3 vein was originally a fault. Deformed clasts and grains of saccharoidal quartz belonging to the previous phase have a cement of microcrystalline quartz. They were observed only in thin sections made from the samples taken from the margin of the K3W vein footwall (Fig. 11j). Tectonic breccia has not been observed at the field scale, but was observed only in thin section. This may be because subsequent hydrothermal brecciation overprints any tectonic breccias formed during earlier shearing.

Host rock deformation

The Karatepe, K3E and Topyurt veins are hosted by QFH porphyry, whereas the other veins are hosted by schist. Deformation of the wall rock hosting each vein was studied in the field and drill core, and is summarized in Table 3. An important observation is that no shear indicator such as slickenlines was seen in the field at the Karatepe vein boundary.

Host rock schist around the NE–SW-trending KK1, KK2, KK3, KK4 and K1 veins does not change foliation orientation adjacent to the veins and these veins have very sharp contacts with their host rock schist as observed in the field and drill cores (Fig. 12). In addition, drill core and grab samples taken from the vein–wall rock contact do not return any shear indicator in petrographic analyses.

In contrast, the schist around the east–west-trending K2 vein is highly fractured, contains hydrothermal quartz veins up to 6–7 cm wide that are discordant to the foliation planes, and the foliation can be observed to bend into the vein (Fig. 13a). In drill cores the wall rock schist of the K3 vein is also intensely fractured and brecciated (Fig. 13b and c). In addition, tectonic breccia with deformed clasts and grains of vein rock was observed at the vein footwall–wall rock contact (Fig. 11j) in the petrographic analyses.

The east–west-striking Karatepe vein, hosted by porphyry, is surrounded by a domain of cemented extensional fractures and a small-scale post-mineralization fault with small displacement (*c.* 1 m) on the Karatepe vein (Fig. 5). Cataclasite is also found at the vein footwall–wall rock contact (Fig. 10) in the petrographic analyses, which is an important shear indicator.

The wall rock zone of the Topyurt vein is also intensely deformed with many extensional veins and hard-silicified resistant porphyry screens (Fig. 7).

Discussion

Kinematics of the vein system

Cataclasite at the margin of the Karatepe vein (of feldspar from wall rock QFH, and chalcedony from the first phase of mineralization) contains asymmetric shear indicators (Fig. 10a), suggesting that the structure hosting the vein is a fault. Hydrothermal quartz forming the Karatepe vein (Fig. 9) and filling the comb fractures around it

Table 3. *Summary of host rock deformation observed around the major quartz veins*

Vein	Host rock	Host rock deformation*
Karatepe	Porphyry	F, V
KK1	Schist	ND
KK2	Schist	ND
KK3	Schist	ND
KK4	Schist	ND
K1	Schist	ND
K2	Schist	FC, V
K3E	Porphyry	F, B, V
K3W	Schist	F, B, V
Topyurt	Porphyry	V

*B, brecciated; F, fractured; FC, foliation changes; ND, not deformed; V, veined.

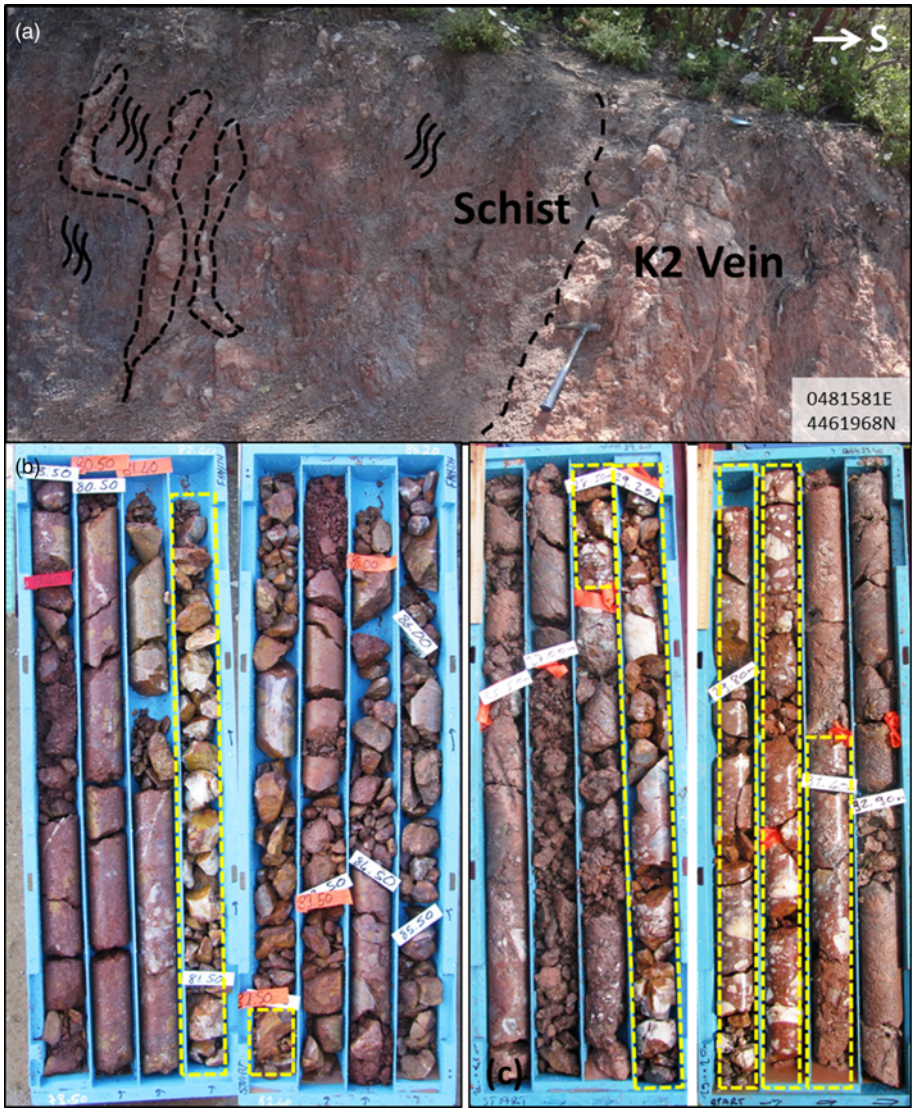

Fig. 13. (**a**) Photograph showing that the schist adjacent to the K2 vein is highly deformed and hosts hydrothermal quartz veins discordant to the foliation planes (wavy black lines represent the orientation of foliation surfaces; black dashed lines represent the boundaries of discordant veins). It should be noted that the foliation surfaces are not continuous and change their attitude. (**b**) Photograph of KED-76 78.5–86.2 m interval core boxes showing that the host rock porphyry is fractured, brecciated and veined around the K3E vein. It should be noted that the porphyry includes the fragments of hydrothermal quartz veinlets around the hanging wall of the vein (dashed lines indicate the vein interval). (**c**) Photograph of KED-20 24.9–33.4 m interval core boxes showing that the host rock schist is highly fractured and brecciated around the K3W vein. It should be noted that the deformation is higher around the hanging wall of the vein, and the schist includes fragments of hydrothermal quartz veinlets around the hanging wall of the vein (dashed lines indicate the vein interval).

(Fig. 5c) shows that these structures formed within the same deformation event. Infill of a comb quartz veinlet adjacent to the Karatepe vein has a granular texture and inequant fabric rather than a fibrous texture (Fig. 6c), which shows that the opening of the fracture was more rapid than the growth of the quartz crystals. We suggest that the brittle fracturing and dilation occurred during co-seismic or post-seismic aftershock phases of an earthquake, and then quartz cement was deposited progressively and sealed the fracture during the passive interseismic phase (e.g. Ramsay 1980; Woodcock *et al.* 2007). Furthermore, comb-textured extension fractures around the Karatepe vein are proximal to the vein margin (Fig. 5b and c), and most of them curve towards the vein. This suggests that they are extensional fractures adjacent to the Karatepe fault that formed after slip on the irregular Karatepe fault plane.

The Karatepe fault-hosted vein is surrounded by extensional veins that have orientations consistent with left-lateral kinematics. We can infer a palaeostress for this subset of structures by assuming that the minor principal stress is perpendicular to the mean orientation of the Karatepe damage zone extensional veins, and their intersection with the fault plane is parallel to the intermediate principal stress. The results of these calculations gives orientations of σ_1, σ_2 and σ_3 of 034°/02°, 124°/59° and 304°/31°, respectively (Fig. 14a and b). Hydrothermal macrocrystalline quartz was also observed in the extensional veins along the river valley similar to those around the Topyurt and Karatepe veins. The consistent textures and orientations of the main veins and sheeted veins suggest that all these veins are related to the same hydrothermal mineralization event. Strikes of all these veins (Fig. 14c) suggest that the horizontal component of the minimum principal stress (σ_3) was N35°W. The Karatepe inferred stress (Fig. 14a) compares well with the extension direction for all the measured extensional veins in the field area (Fig. 14c).

Similar analyses cannot be conducted for K2 and K3 veins. Although the drill cores show that K2 and K3 have extensional veins in the damage zone, they are not exposed at the surface, so their orientations cannot be measured. The K2 and K3 veins are dipping to the north, opposite to Karatepe, but if they were active in the same stress field they too would have a component of left-lateral slip. In the absence of a more complete dataset (for instance, through oriented drill core) it is not possible to conduct a more sophisticated palaeostress analysis, but the structures all seem consistent with subhorizontal NE–SW σ_1.

The tilt on the younger sediments means that the older veins must also have been tilted. However, it is not straightforward to relate untilted stress orientations to tectonics because (1) there may be unmapped faults that tilt different blocks in the younger sediments, (2) previous tilting may have affected the block of mineralized veins before the formation of the unconformity and (3) Late Miocene aged vertical-axis rotations (Kaymakci *et al.* 2007) must also be considered in reconstructing the palaeostresses responsible for the geothermal system, although the amount of such vertical-

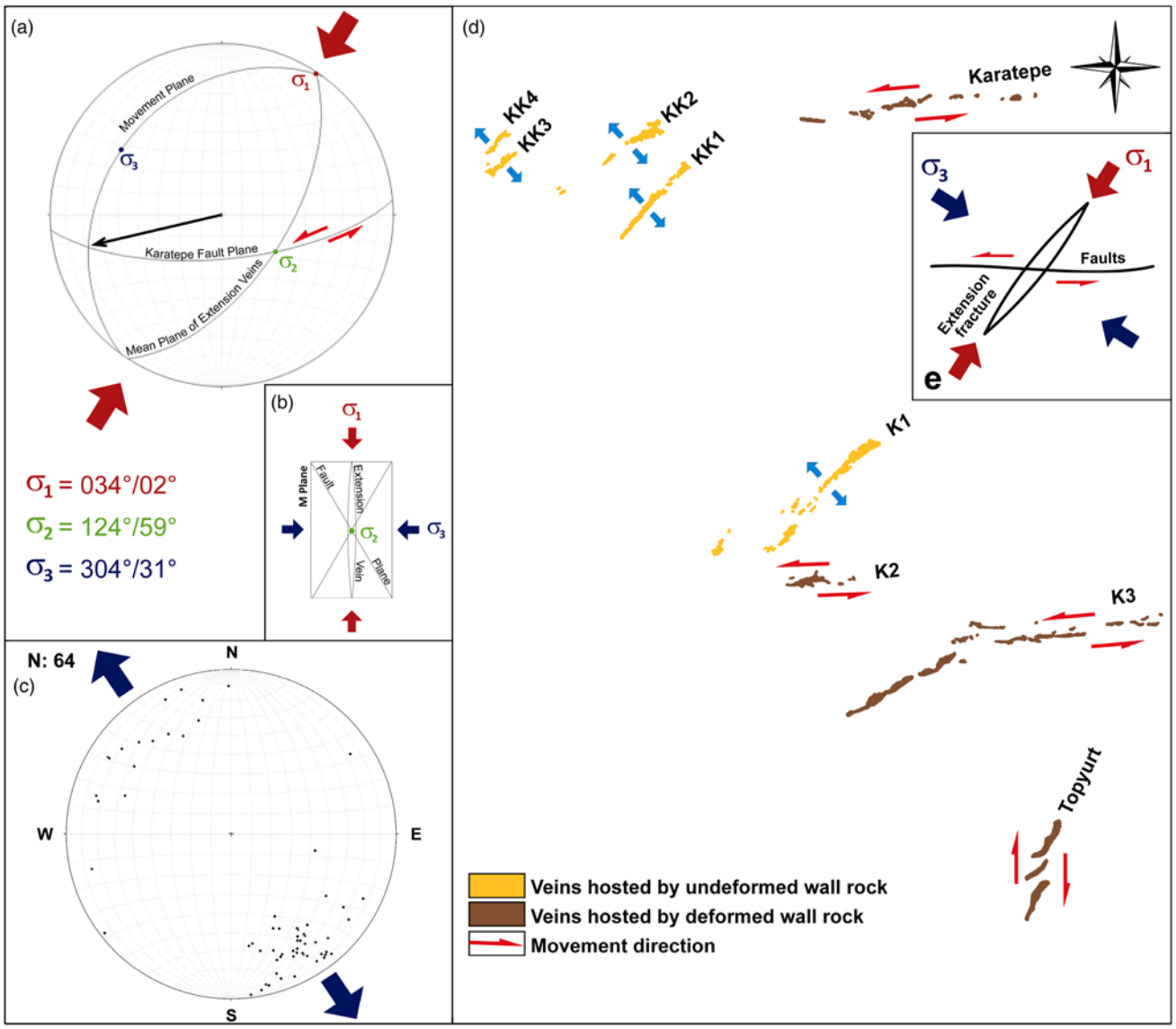

Fig. 14. (**a**) Determination of principal stress orientations based on Anderson's theory of faulting by plotting the plane representing the mean orientation of the Karatepe vein and the mean plane of the adjacent extensional veins on an equal area stereonet based on the assumptions that (1) the minor principal stress (σ_3) is perpendicular to the extensional veins, and (2) their intersection with the fault plane is parallel to the intermediate principal stress (σ_2). (**b**) A hypothetical diagram showing the relationship between the principal stress directions and opening of the veins and movement along the fault plane (M plane is the movement plane). (**c**) Poles to all the extensional veins in the Kestanelik deposit plotted on an equal-area stereonet with arrows indicating the opening direction for the veins. (**d**) A sketch model showing the kinematics of the major quartz veins at Kestanelik based on the determined principal stress directions. (**e**) A hypothetical model showing the opening of the structures hosting the Kestanelik major quartz veins.

axis rotations is very difficult to contrain because of the large error ranges in the palaeomagnetic measurements. Instead, we want to establish if the vein sets are consistent with formation in a single stress regime.

The inferred directions of the principal stresses indicate that the east–west-trending Karatepe, K3 and K2 veins can be characterized as left lateral strike-slip faults, whereas the NE–SW-trending KK1, KK2, KK3, KK4 and K1 veins are extensional (Mode I) fractures (Figs 14d, e and 15). In addition, the NE–SW-trending Topyurt vein and associated north–south-trending zone of wall rock veins correspond to a right lateral en echelon brittle shear zone (Fig. 14d and e). Although kinematic indicators could not be found for the fault-hosted veins, sheared cataclasite, tectonic breccia and intensely deformed characteristics of the wall rocks suggest that they are developed as a result of shearing. However, the NE–SW-trending KK1, KK2, KK3, KK4 and K1 veins do contain evidence of extensional fracturing (Mode I opening) and lack any shear indicators and wall rock deformation.

Permeability enhancement and fluid flow

Integration of the data from the Kestanelik epithermal vein system and the review of the literature suggest that three permeability enhancement and fluid flow mechanisms could have been active in the Kestanelik epithermal gold deposit.

Co-seismic rupturing

Co-seismic rupturing generates permeable pathways, which are clogged progressively by interseismic hydrothermal sealing. Sibson (1987) suggested that episodic fault rupture causes co-seismic dilation at the rupture zones and an associated fluid pressure drop. The co-seismic fluid pressure drop drives boiling, which is evidenced by the common occurrence of pseudo-bladed quartz and crackle breccia in the Kestanelik veins. Rapid closure of permeability by hydrothermal precipitation clogs pathways and results in local pressure build-up. Quartz–iron oxide cement within the breccias shows that ascending boiled fluid may also have mixed

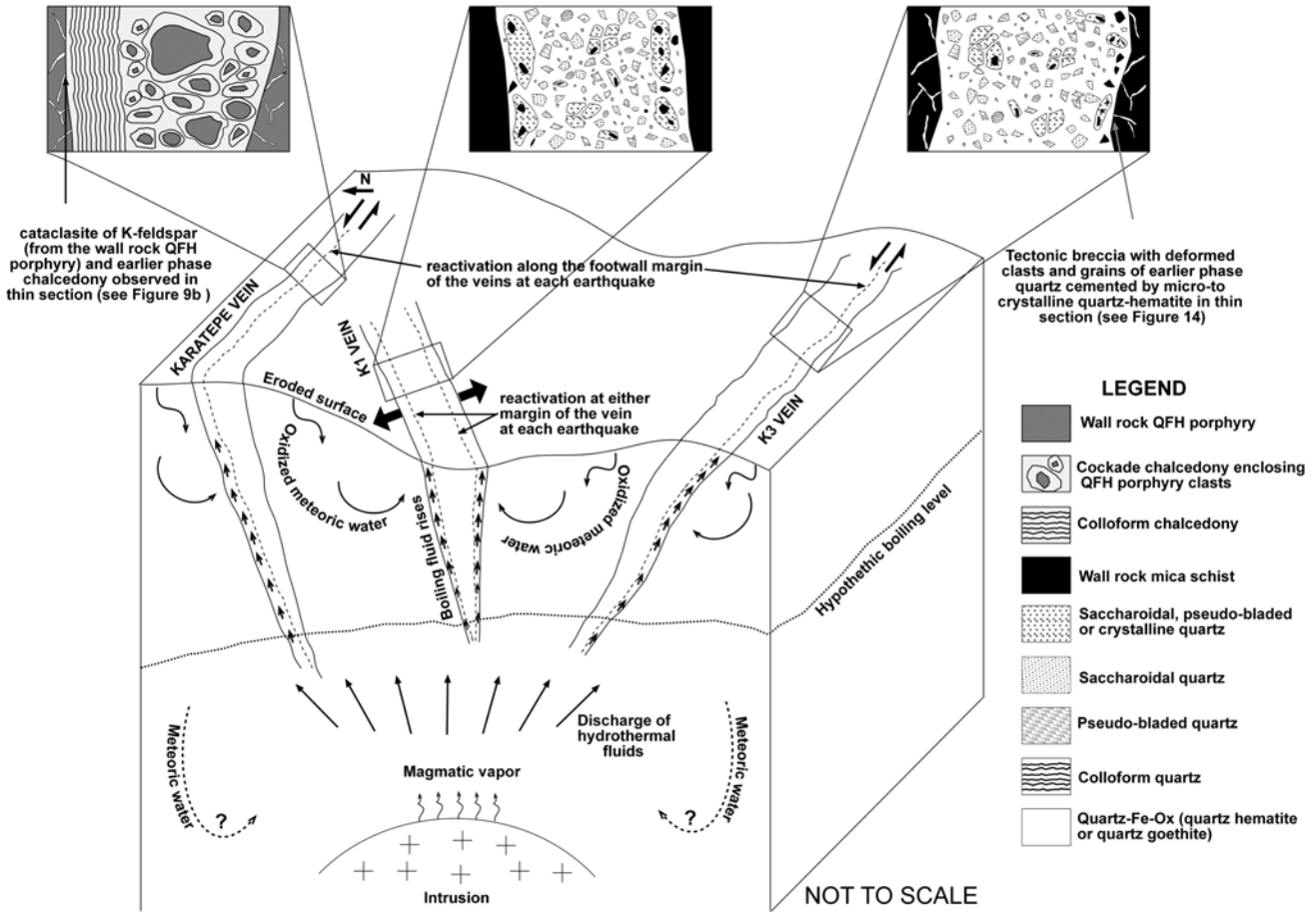

Fig. 15. A conceptual model for the repeated reactivation and opening of clogged veins and associated fluid flow, mineralization and resulting vein textures at Kestanelik. It should be noted that the K3 vein represents the fault-hosted veins (except the Karatepe vein), whereas the K1 vein represents the extensional (Mode I) fracture-hosted veins of the Kestanelik.

with descending oxidized surface meteoric water in the shallower parts of the system (Fig. 15). Salinity and homogenization temperature data from fluid inclusion analyses along with the O and H stable isotope analyses of fluid inclusions could be used to further constrain boiling and mixing events.

Shear indicators, such as cataclasite and tectonic breccia cemented by a later phase of silicification, are observed at the footwall of the vein–wall rock contacts of the Kestanelik fault-hosted veins. These and the presence of angular wall rock clasts at the margins of extensional (Mode I) fractures suggest rupturing along the fault planes and extensional fractures (Fig. 15).

The inequigranular infill of a comb quartz veinlet at the wall rock of the Karatepe vein shows that the opening of the fracture was more rapid than the growth of the quartz crystals. This texture is more consistent with the brittle fracturing and dilation occurring during co-seismic or post-seismic aftershock phases of an earthquake than with progressive silicification to seal the fracture during the passive interseismic phase (Woodcock *et al.* 2007). In addition, the absence of any grading in the clasts of the cockade breccias of the Karatepe vein (Fig. 9) may indicate that both shaking (where brecciation occurs owing to seismic faulting and clasts are cemented during interseismic period) and fluidization (see below) may have played a role in the formation of the cockade breccias (see Frenzel & Woodcock 2014): these represent the first phase of fluid flow and formation of the Karatepe vein.

Hydraulic fracturing

Rapid hydrothermal sealing of the pathways by mineral deposition could cause an increase in hydrothermal fluid pressure. Increase in fluid pressure may promote extensional-shear failure of the vein walls at depth, and the veins are subsequently propagated upwards into the shallowest part of the crust. Provided that the pore fluid factor increases at rates higher than the increase in stress difference (Cox 2005), when the hydrothermal fluid pressure exceeds the combined minimum principal stress (σ_3) and the tensile strength of the cap rock (T), then hydraulic fracturing occurs (Phillips 1972). This triggers boiling owing to pressure release and creates permeable structural conduits for the input of fluids, and results in formation of hydrothermal crackle breccias without significant rotation of the fragments (Jébrak 1997). The cements have to be very rapidly deposited or the clasts would settle out causing grading and/or rotation. Crackle breccias with fragments of the early quartz infill without significant rotation cemented by later quartz or quartz iron–oxide forming a network of veinlets observed at Kestanelik veins (Fig. 11e–g) indicate dilatant fracturing with a negligible shear component and suggest that hydraulic fracturing may have occurred at the main vein conduits. As discussed above, the absence of any grading may indicate fluidization, where brecciation occurs as a result of hydraulic fracturing and subsequent fluid flow cements the clasts (Frenzel & Woodcock 2014).

Transient local stress variation

Local stress orientation can change transiently, resulting in permeability enhancement. Intrusion of dykes coeval with the gold mineralization at Kestanelik (Fig. 3), and the dynamic nature of the geothermal systems, may explain the transient kinematic variation by disrupting the local stress field and triggering earthquakes (Fukuyama *et al.* 2001; Toda *et al.* 2002; Waite &

Smith 2002; Micklethwaite 2009). Transient local stress variation might enhance permeability along the corrugated strike of the Kestanelik structures by facilitating slip on misoriented surfaces and influencing the kinematics of the structures. In addition, locations where the dip changes in the Kestanelik structures have potential to enhance permeability, as they lead to stress concentrations and localize intense deformation compared with the smooth and planar segments (Cox 2005) during earthquakes. It is important to note that permeability and fluid flow will be intermittent in both cases.

Conceptual model for the evolution of the Kestanelik veins

On the basis of field, drill hole and microstructural observations we suggest that the dominant mechanism for formation of the vein textures was co-seismic rupturing (Fig. 15). When an earthquake occurred, east–west-trending fault-hosted veins reactivated and opened along their footwall–wall rock contacts. Conversely, NE–SW-trending Mode I fracture-hosted veins reactivated and opened along either margin. Coseismic rupture and dilation resulted in rapid fluid pressure drop and drove boiling of hydrothermal fluids. Boiling fluid rose along the newly created permeable pathways and may have mixed with descending oxidized surface meteoric water in the shallower parts of the system. The evidence for rupture along the walls of the veins includes the following: shear indicators such as cataclasite and tectonic breccia of wall rock; pre-existing vein infill cemented by a later phase of silicification observed at the footwall of the vein–wall rock contacts of two of the fault-hosted veins (Karatepe and K3 veins); the presence of angular wall rock clasts at the margins of extensional (Mode I) fractures. Evidence for multiple brecciation and sealing events consists of chaotic breccias with polymictic clasts from pre-existing vein infill and clasts of wall rock cemented by quartz–hematite or quartz–goethite. This evidence suggests repeated reactivation and opening in subsequent co-seismic events. Crackle breccias are evidence that hydraulic fracturing may also have taken place.

Although none of the fault rock textures that have been observed are definitely diagnostic of dynamic rupture, it is not possible to exclude dynamic slip (Cowan 1999; Rowe & Griffith 2015). However, it has been documented that earthquake rupturing can induce opening of faults and fractures off the plane of the main fault (Micklethwaite & Cox 2004, 2006). Kestanelik was likely to have been an earthquake-prone region in the Late Eocene at the time of mineralization because of the tectonic activity caused by further convergence after the closure of the northern branch of the Neo-Tethys Ocean (Late Cretaceous–Early Eocene: Şengör & Yilmaz 1981; Okay & Tüysüz 1999; Sherlock *et al.* 1999; Önen & Hall 2000; Kaymakci *et al.* 2007, 2009). In addition, it is well known that geothermal regions are dynamic, and that pressure transfer owing to hydrothermal flow and mineralization can induce seismicity (e.g. Hill 1977).

As noted above, the altered porphyry zone is wider than usually expected for structurally controlled alteration. It is possible that this wide halo is further evidence for multiple recharge events of the altering fluids through repeated rupture of the main veins, and more protracted flow within the damage zone veins.

Implications for prospect evaluation

Mapping and study of veins and wall rock veins, and collection of structural data on the veins are powerful tools to unravel the kinematics of the vein system. Correlation of the kinematics of the mineralized or high-grade vein system along with timing of the mineralization may help in the search for areas or targets by defining the favourable orientation of structures for mineralization. Because repeated boiling results in multiple overprinting of textures, key features such as the shear textures may be missed if only a limited number of outcrops or drill cores are examined; therefore comprehensive petrographic investigation of vein material and delineation of the ore-vein textures addressing multiple boiling and silicification phases (especially close to the vein margins) is strongly advised. The understanding of textures showing clogging and subsequent boiling of the hydrothermal systems in correlation with structural easement or enhancement of fluid flow along the conduits may contribute to target assessment in epithermal systems as gold precipitation is triggered by boiling and oxidation in low-sulphidation epithermal gold deposits. Thus mapping and petrographical analysis of the ore-vein textures both on the outcrops and in drill cores together with the geochemical analysis of gold assay data help us to understand not only the likely gold deposition mechanism(s) but also the potential gold distribution within the deposits.

Conclusions

The Kestanelik fracture system is an LS epithermal gold deposit evident from pseudo-bladed quartz, colloform to crustiform quartz, comb to cockade ore-vein textures and hydrothermal breccias. The mineralization is hosted by major quartz veins up to 13.6 m thick, as well as sheeted extensional quartz veins in the Kestanelik River valley and extensional wall rock veins surrounding the major quartz veins. Vein textures and breccias are indicative of repeated sealing and subsequent brecciation of wall rock and the pre-existing vein infill. Boiling and fluid mixing are likely mechanisms of gold deposition. According to the field and petrographic data, the kinematics of the vein system is consistent with formation in a single regional stress field: east–west-trending veins are characterized as left lateral faults, whereas NE–SW-trending veins are characterized as extensional (Mode I) fractures. The gold grade is higher in the extensional veins, although further detailed analysis of the vein textures is required to unpick the mechanism(s) of gold deposition.

Cataclastic deformation and tectonic brecciation of wall rocks and early quartz, hydrothermal crackle breccias and matrix-supported chaotic breccias of pre-existing vein infill, all of which are cemented by late iron-oxide-bearing quartz, indicate that co-seismic rupturing and hydraulic fracturing are two major permeability enhancement mechanisms that would have caused repeated reactivation of clogged permeable pathways at Kestanelik. Additionally, transient local stress variation, caused by syn-mineralization dyke intrusion, has the potential to enhance permeability on misoriented surfaces and at locations where the dip changes on vein planes. These results indicate that a thorough understanding of structural geology and kinematics, when coupled with the examination of evidence for boiling and other mineralization mechanisms, should be an important tool in defining ore zones within areas of mineralization in epithermal gold deposits.

Acknowledgements This work is a part of a PhD study carried out at the University of Strathclyde with University of Strathclyde scholarship and financial support of Geochemico Incorporated. J. Cosgrove and S. Micklethwaite are thanked for their constructive reviews of the paper. The authors acknowledge Chesser Resources for providing accommodation and logistics for fieldwork, and access to the drill core data. We gratefully thank C. S. Yüceer, M. Çetintas, and geologists and staff at Kestanelik for their generous help in all phases of the fieldwork. We also would like to thank E. Özcan for biostratigraphical age determinations of Eocene units. This paper is dedicated to the memory of David Robert Gladwell.

Funding N.G. is grateful to the University of Strathclyde for funding the PhD. The authors are grateful to the Geochemico Incorporated for financial support.

Scientific editing by Karel Schulmann

References

Allmendinger, R.W., Cardozo, N.C. & Fisher, D. 2013. *Structural Geology Algorithms: Vectors and Tensors*. Cambridge University Press, Cambridge.

Altunkaynak, Ş. & Genç, Ş.C. 2008. Petrogenesis and time-progressive evolution of the Cenozoic continental volcanism in the Biga Peninsula, NW Anatolia (Turkey). *Lithos*, **102**, 316–340.

Buchanan, L.J. 1981. Precious metal deposits associated with volcanic environments in the southwest. *In*: Dickson, W.R. & Payne, W.D. (eds) *Relations of Tectonics to Ore Deposits in the Southern Cordillera*. Arizona Geological Society Digest, **14**, 237–262.

Burnside, N.M., Shipton, Z.K., Dockrill, B. & Ellam, R.M. 2013. Man-made versus natural CO_2 leakage: a 400 k.y. history of an analogue for engineered geological storage of CO_2. *Geology*, **41**, 471–474.

Caine, J., Evans, J. & Forster, C. 1996. Fault zone architecture and permeability structure. *Geology*, **24**, 1025–1028.

Cardozo, N. & Allmendinger, R.W. 2013. Spherical projections with OSXStereonet. *Computers and Geosciences*, **51**, 193–205.

Cowan, D.S. 1999. Do faults preserve a record of seismic slip? A field geologist's opinion. *Journal of Structural Geology*, **21**, 995–1001.

Cox, S. 2005. Coupling between deformation, fluid pressures, and fluid flow in ore-producing hydrothermal systems at depth in the crust. *Economic Geology*, **100**, 39–75.

Cox, S., Knackstedt, M. & Braun, J. 2001. Principles of structural control on permeability and fluid flow in hydrothermal systems. *Reviews in Economic Geology*, **14**, 1–24.

Curewitz, D. & Karson, J.A. 1997. Structural settings of hydrothermal outflow: fracture permeability maintained by fault propagation and interaction. *Journal of Volcanology and Geothermal Research*, **79**, 149–168.

Davatzes, N.C., Eichhubl, P. & Aydin, A. 2005. Structural evolution of fault zones in sandstone by multiple deformation mechanisms: Moab fault, southeast Utah. *Geological Society of America Bulletin*, **117**, 135–148.

Dong, G., Morrison, G. & Jaireth, S. 1995. Quartz textures in epithermal veins, Queensland—classification, origin, and implication. *Economic Geology*, **90**, 1841–1856.

Fournier, R.O. 1989. Geochemistry and dynamics of the Yellowstone National Park hydrothermal system. *Annual Review of Earth and Planetary Sciences*, **17**, 13–53.

Frenzel, M. & Woodcock, N.H. 2014. Cockade breccia: product of mineralisation along dilational faults. *Journal of Structural Geology*, **68**, 194–206.

Fukuyama, E., Kubo, A., Kawai, H. & Nonomura, K. 2001. Seismic remote monitoring of stress field. *Earth, Planets and Space*, **53**, 1021–1026.

Hedenquist, J.W. 2011. Observations on the Kestanelik and Karaayi prospects, Biga Peninsula, Turkey. Unpublished report for Chesser Resources.

Hedenquist, J.W. & Lowenstern, J.B. 1994. The role of magmas in the formation of hydrothermal ore deposits. *Nature*, **370**, 519–527.

Hedenquist, J.W., Arribas, M.A. & Gonzalez-Urien, E. 2000. Exploration for epithermal gold deposits. *Reviews in Economic Geology*, **13**, 245–277.

Henley, R.W. 1985. The geothermal framework of ephithermal deposits. *Reviews in Economic Geology*, **2**, 1–24.

Hill, D.P. 1977. A model for earthquake swarms. *Journal of Geophysical Research*, **82**, 1347–1352.

Hulin, C.D. 1929. Structural control of ore deposition. *Economic Geology*, **24**, 15–49.

Jébrak, M. 1997. Hydrothermal breccias in vein-type ore deposits: a review of mechanisms, morphology and size distribution. *Ore Geology Reviews*, **12**, 111–134.

Kaymakci, N., Aldanmaz, E., Langereis, C., Spell, T.L., Gurer, O.F. & Zanetti, K.A. 2007. Late Miocene transcurrent tectonics in NW Turkey: evidence from palaeomagnetism and ^{40}Ar–^{39}Ar dating of alkaline volcanic rocks. *Geological Magazine*, **144**, 379–392.

Kaymakci, N., Özcelik, Y., White, S.H. & Van Dijk, P.M. 2009. Tectono-stratigraphy of the Çankiri Basin: Late Cretaceous to Early Miocene evolution of the Neotethyan Suture Zone in Turkey. *In*: Van Hinsbergen, D.J.J., Edwards, M.A. & Govers, R. (eds) *Geodynamics of Collision and Collapse at the Africa–Arabia–Eurasia Subduction Zone*. Geological Society, London, Special Publications, **311**, 67–106, https://doi.org/10.1144/SP311.3

Lalou, C., Reyss, J.L., Brichet, E., Arnold, M., Thompson, G., Fouquet, Y. & Rona, P.A. 1993. New age data for Mid-Atlantic Ridge hydrothermal sites: TAG and Snakepit geochronology revisited. *Journal of Geophysical Research*, **98**, 9705–9713.

Micklethwaite, S. 2009. Mechanisms of faulting and permeability enhancement during epithermal mineralisation: Cracow goldfield, Australia. *Journal of Structural Geology*, **31**, 288–300.

Micklethwaite, S. & Cox, S. 2004. Fault-segment rupture, aftershock-zone fluid flow, and mineralisation. *Geology*, **32**, 813–816.

Micklethwaite, S. & Cox, S. 2006. Progressive fault triggering and fluid flow in aftershock domains: examples from mineralized Archean fault systems. *Earth and Planetary Science Letters*, **250**, 318–330.

Micklethwaite, S., Sheldon, H.A. & Baker, T. 2010. Active fault and shear processes and their implications for mineral deposit formation and discovery. *Journal of Structural Geology*, **32**, 151–165.

Okay, A.I. & Tüysüz, O. 1999. Tethyan sutures of northern Turkey. *In*: Durand, B., Jolivet, L., Horváth, F. & Séranne, M. (eds) *The Mediterranean Basins: Tertiary Extension within the Alpine Orogen*. Geological Society, London, Special Publications, **156**, 475–515, https://doi.org/10.1144/GSL.SP.1999.156.01.22

Okay, A.I., Siyako, M. & Bürkan, K.A. 1990. Geology and tectonic evolution of the Biga Peninsula. *Bulletin of the Turkish Association of Petroleum Geologists*, **2**, 83–121 [in Turkish].

Okay, A.I., Satır, M., Maluski, H., Siyako, M., Monie, P., Metzger, R. & Akyüz, S. 1996. Paleo- and Neo-Tethyan events in northwest Turkey: geological and geochronological constraints. *In*: Yin, A. & Harrison, M. (eds) *Tectonics of Asia*. Cambridge University Press, Cambridge, 420–441.

Önen, P. & Hall, R. 2000. Sub-ophiolite metamorphic rocks from NW Anatolia, Turkey. *Journal of Metamorphic Geology*, **18**, 483–495.

Phillips, W.J. 1972. Hydraulic fracturing and mineralisation. *Journal of the Geological Society, London*, **128**, 337–359, https://doi.org/10.1144/gsjgs.128.4.0337

Ramsay, J. 1980. The crack-seal mechanism of rock deformation. *Nature*, **284**, 135–139.

Rowe, C.D. & Griffith, W.A. 2015. Do faults preserve a record of seismic slip: a second opinion. Invited Review. *Journal of Structural Geology*, **78**, 1–26.

Rowland, J.V. & Sibson, R.H. 2004. Structural controls on hydrothermal flow in a segmented rift system, Taupo Volcanic Zone, New Zealand. *Geofluids*, **4**, 259–283.

Sanchez-Alfaro, P., Reich, M. *et al.* 2016. The optimal windows for seismically-enhanced gold precipitation in the epithermal environment. *Ore Geology Reviews*, **79**, 463–473.

Schöpfer, M.P.J., Childs, C. & Walsh, J.J. 2006. Localisation of normal faults in multilayer sequences. *Journal of Structural Geology*, **28**, 816–833.

Schöpfer, M.P.J., Childs, C., Walsh, J.J., Manzocchi, T. & Koyi, H.A. 2007. Geometrical analysis of the refraction and segmentation of normal faults in periodically layered sequences. *Journal of Structural Geology*, **29**, 318–335.

Şengör, A.M.C. & Yilmaz, Y. 1981. Tethyan evolution of Turkey: a plate tectonic approach. *Tectonophysics*, **75**, 181–241.

Sherlock, S., Kelley, S., Inger, S., Harris, N. & Okay, A.I. 1999. ^{40}Ar–^{39}Ar and Rb/Sr geochronology of high-pressure metamorphism and exhumation history of the Tavsanli Zone, NW Turkey. *Contributions to Mineralogy and Petrology*, **137**, 46–58.

Sibson, R.H. 1987. Earthquake rupturing as a mineralizing agent in hydrothermal systems. *Geology*, **15**, 701–704.

Sillitoe, R.H. 2010. Porphyry copper systems. *Economic Geology*, **105**, 3–41.

Sillitoe, R.H. & Hedenquist, J.W. 2003. *Linkages between Volcanotectonic Settings, Ore-fluid Compositions, and Epithermal Precious Metal Deposits*. Society of Economic Geologists, Special Publications, **10**.

Simmons, S.F., White, N.C. & John, D. 2005. Geological characteristics of epithermal precious and base metal deposits. *Economic Geology, 100th Anniversary Volume*, 485–522.

Spurr, J.E. 1925. Ore magmas versus magmatic waters. *Engineering and Mining Journal*, **119**, 890.

Toda, S., Stein, R.S. & Sagiya, T. 2002. Evidence from the AD 2000 Izu islands earthquake swarm that stressing rate governs seismicity. *Nature*, **419**, 58–61.

Türkecan, A. & Yurtsever, A. 2002. *1:500 000 Scale Geological Map of Turkey, İstanbul Sheet*. General Directorate of Mineral Research and Exploration Publications, Ankara.

Ünal-İmer, E., Gulec, N., Kuscu, I. & Fallick, A.E. 2013. Genetic investigation and comparison of Kartaldag and Madendag epithermal gold deposits in Canakkale, NW Turkey. *Ore Geology Reviews*, **53**, 204–222.

Waite, G.P. & Smith, R.B. 2002. Seismic evidence for fluid migration accompanying subsidence of the Yellowstone caldera. *Journal of Geophysical Research*, **107**, 2177.

White, N.C. & Hedenquist, J.W. 1990. Epithermal environments and styles of mineralisation: variations and their causes, and guidelines for exploration. *Journal of Geochemical Exploration*, **36**, 445–474.

White, N.C. & Hedenquist, J.W. 1995. Epithermal gold deposits: styles, characteristics and exploration. *Society of Economic Geologists Newsletter*, **23**, 9–13.

Woodcock, N.H., Dickson, J.A.D. & Tarasewicz, J.P. 2007. Transient permeability and reseal hardening in fault zones: evidence from dilation breccia textures. *In*: Lonergan, L., Jolley, R.J.H., Rawnsley, K. & Sanderson, D.J. (eds) *Fractured Reservoirs*. Geological Society, London, Special Publications, **270**, 43–53, https://doi.org/10.1144/GSL.SP.2007.270.01.03